High-Heat Flux Testing of Irradiated Tungsten based Materials for Fusion Applications using Infrared Plasma Arc Lamps

*Adrian S. Sabau¹, Evan K. Ohriner¹, Jim Kiggans¹, Charles R. Schaich², Yoshio Ueda³, David C. Harper¹, Yutai Katoh¹, Lance L. Snead¹, and Thak S. Byun¹

¹Materials Science and Technology Division
Oak Ridge National Laboratory, Oak Ridge, TN 37831

²Energy & Transportation Science Division
Oak Ridge National Laboratory, Oak Ridge, TN 37831

³Graduate School of Engineering, Osaka University 2-1 Yamadaoka, Suita, Osaka 565-0871, Japan

*corresponding author: Adrian S. Sabau (<u>sabaua@ornl.gov</u>) Ph: (865) 241-5145 Fax: (865) 574-4357

ICFRM-16 abstract number: 16-296

ici kwi-10 abstract number. 10-270

Abstract

Testing of advanced materials and component mock-ups under prototypical fusion high-heat flux conditions, while historically a mainstay of fusion research has proved challenging, especially for irradiated materials. A new high-heat flux testing facility based on water-wall Plasma Arc Lamps (PALs) is now introduced for materials and small component testing. Two PAL systems, utilizing a 12,000 °C plasma arc contained in a quartz tube cooled by a spiral water flow over the inside tube surface, are currently in use. The first PAL system provides a maximum incident heat flux of 4.2 MW/m² over an area of 9x12 cm². The second PAL available at ORNL provides a maximum incident heat flux of 27 MW/m² over an area of 1x10 cm². The absorbed heat fluxes into a tungsten target for the two PALs are approximately 1.97 and 12.7 MW/m², respectively.

This paper will present the overall design of the new PAL facilities as well as the design and implementation of the Irradiated Material Target Station (IMTS). The IMTS is primarily designed for testing the effects of heat flux or thermal cycling on material coupons of interest, such as those for plasma facing components. Moreover, IMTS designs are underway to extend the testing of small mock-ups for assessing the combined heating and thermomechanical effects of cooled, irradiated components. For the testing of material "coupons", the specimens are placed in a shallow recess within the molybdenum holder that is attached to a water-cooled copper alloy rod. As the measurement of the temperature for thin specimens during PAL operation is challenging since traditional approaches of temperature measurement cannot be employed due to the infrared heating and proximity of the PAL reflector to the specimen that does not allow a direct line of site, experiments for temperature calibration are presented. Temperature results were shown for thermal cycling under high-heat flux testing of tungsten coupon specimens that were neutron irradiated in the HFIR reactor. Radiological surveys indicated minimal contamination of the 36x36x18 cm test section, demonstrating the capability of the new facility to handle irradiated specimens at high temperature.

Keywords: high-heat flux testing, tungsten, infrared, arc-lamp, divertor

Notice: This submission was sponsored by a contractor of the United States Government under contract DE-AC05-00OR22725 with the United States Department of Energy. The United States Government retains, and the publisher, by accepting this submission for publication, acknowledges that the United States Government retains, a nonexclusive, paid-up, irrevocable, worldwide license to publish or reproduce the published form of this submission, or allow others to do so, for United States Government purposes.

Abbreviations

DEMO – DEMOnstration Power Plant

HHFT – high-heat flux testing

HFIR – High Flux Isotope Reactor

IMTS – Irradiated Material Target Station

ITER – International Thermonuclear Experimental Reactor

PAL – Plasma Arc Lamps

1. Introduction

Developing plasma-facing materials is a key challenge to the realization of the steady state high power fusion that will be required in DEMO and future fusion power plants. Material characterization of divertor armor includes the testing of actively cooled components under fusion specific heat flux loading conditions at operational temperatures. Operational conditions include surface temperatures of 1,300 °C and higher and back-side component temperature of 500 to 700°C [1-3]. Static heat loads corresponding to cycling loads during normal operation, are estimated to be up to 20 MW/m² in the divertor targets in ITER. High heat flux testing in electron beam facilities, particle beam facilities, infrared heater and in-pile tests have been performed [1]. It is a challenge to expose non-irradiated divertor armor materials to high-heat flux that would mimic those in fusion reactors. The intense electron or hydrogen ion beams must be used in pulsed and/or scanned modes to simulate the thermal loads, which are expected during operation [1]. As mechanical properties are affected by irradiation [4-8], it is imperative to conduct high-heat flux testing (HHFT) of irradiated materials, as well.

To date, high-heat flux testing (HHFT) has been conducted essentially on non-irradiated specimens due to the difficulty in working with radioactive specimens, such as ensuing instrument contamination. This paper describes HHFT conducted using the plasma arc lamp facilities at Oak Ridge National Laboratory (ORNL), in which the high-heat fluxes are provided by water-wall Plasma Arc Lamps (PALs). Two PALs currently available at ORNL provide fusion-prototypical steady state heat flux conditions; one produces a maximum incident heat flux of 27 MW/m² over a heated area of 1cmx10 cm; the other system produces 4.2 MW/m² over an area up to 9cmx12 cm. The duration of HHFT can be set to any value from 0.02 to 30 s and is limited by the electrode and reflector coolant; with the additional on-going expansion, the maximum duration of HHFT will be increased from 30 to 450s. These photon-based heat flux sources at ORNL were used previously used for testing of tungsten coatings bonded to F82H steel at high-heat fluxes greater than 10 MW/m² for one thousand cycles at ORNL [9, 10]. Recently, this facility was upgraded based on radiation safety considerations and testing capabilities were illustrated using non-irradiated tungsten specimens as a step toward testing irradiated tungsten specimens [11]. The components of the test chamber were also designed to accommodate materials compatibility requirements posed by high-temperature exposure of lowlevel irradiated tungsten articles, such as release of tungsten oxide. The chamber design will

allow the high-heat flux testing of typical divertor mock-up components with active surface dimensions of 14 cm x14 cm, anticipated for future projects. Issues related to the operation and temperature measurements during testing are presented and discussed. Special consideration was given to thin specimens, which are typical used for investigating the neutron irradiation effects in high activity materials, such as tungsten, as they can be cost effective irradiated in rabbit capsules in nuclear reactors, such as HFIR at ORNL. Results of high-heat flux testing of low-levels irradiated tungsten articles are presented, demonstrating the readiness of the new facility for irradiated specimens.

2. Materials

2.1. Materials and properties

Tungsten specimens were chosen for this study, as tungsten alloys are good candidate materials for plasma-facing components as they exhibit high melting temperature, low vapor pressure, and relatively good thermal conductivity. However, monolithic tungsten has application issues, both in terms of base manufacturability and in as-irradiated properties. Most common forms of tungsten are quite brittle [12, 13], which makes them difficult to form, join, and reliably design with. In the high heat flux application being considered here, maximum tungsten temperatures in excess of 1,000°C are anticipated. In this temperature range, recrystallization of tungsten and its associated grain boundary embrittlement can occur, resulting in loss of ductility at low temperatures. Pure tungsten materials have a recrystallization temperature in the range of 1,150-1,350°C, dependent on the level of work, amount of impurities, grain size [14]. The tungsten crystal, as typical of bcc metals, loses the ability to plastically deform following modest neutron irradiation. As the homologous temperature in fusion application is low for tungsten (even at 1000°C) embrittlement is anticipated to occur at an even more rapid rate [7]. Moreover, monolithic tungsten forms suffer from grain-boundary-induced embrittlement under irradiation [4-8, 15, 16].

2.2. Specimen description

Commercially pure tungsten foil was selected for this study. The source, fabrication, and properties of the tungsten foil (0.5x5x15 cm) used in this study were described in [17]. Two specimens were irradiated at HFIR under the following conditions:

- (a) specimen S1 was in recrystallized condition (1 hour at 2000 $^{\circ}$ C): 80 $^{\circ}$ C (nominal), fast fluence 10^{24} n/m² (E > 0.1 MeV), yielding ~0.02-0.04 dpa in tungsten, and
- (b) specimen S2 was in as-rolled condition: 80 $^{\circ}$ C (nominal), fast fluence $2x10^{23}$ n/m 2 (E >
- 0.1 MeV), yielding ~0.004-0.008 dpa in tungsten.

For the recrystallized condition the grain size is not expected to change during heat flux testing or radiation exposure. Micrographs of the two irradiated specimens following neutron irradiation but prior to the HHFT were taken at a magnification of 1,000X with a VHX-1000 Keyence optical microscope and are shown in Figure 1.

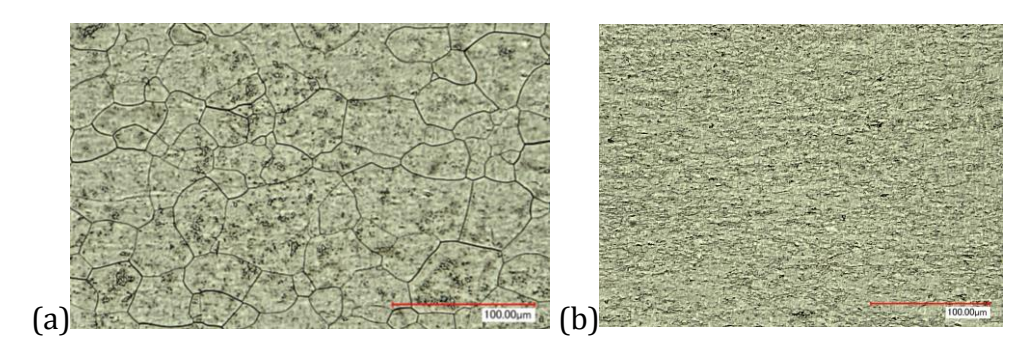


Figure 1. Micrographs of the two specimens following neutron irradiation but before HHFT: (a) recrystallized tungsten foil (Specimen S1) and (b) as-rolled tungsten foil (Specimen S2).

2 Experimental Method

2.1 Plasma-arc-lamps facility, incident heat flux, and optical properties

The water-wall plasma arc lamp was developed at the University of British Columbia where a key innovation was to protect the quartz glass tube from overheating by the 12,000 °C temperature of the arc with a layer of water flowing in a spiral on the inside surface of the tube [18, 19]. Deionized water mixed with argon or nitrogen gas enters at the cathode side through high-velocity jets impinging at a given angle, spiraling around the length of the quartz tube in a

uniform 2-3 mm thick film, cooling the quartz wall and removing any tungsten particulates that may be expelled from the electrodes. The gas flows in a spiral fashion through the center of the tube, and a capacitive circuit initiates the plasma. A water-cooled and highly polished line focus reflector redirects the radial radiant energy output to the specimen being processed [20].

A comparison with the other established heat sources for high-heat flux testing facilities was discussed in [11], where differences in the penetration depth and surface area coverage were highlighted. The illumination distance between the reflector bottom surface and specimen surface at which maximum heat flux would be attained is 2 cm [21]. At highest power, the spectrum of the PAL is concentrated at [0.2:1.4] μ m [11, 22]. Spectral dependence of optical properties must be considered to estimate the absorbed energy in tungsten exposed to plasma arc lamp. Based on Kirckoff's law, the absorptivity is equal to emissivity. An overall emissivity, e_{PAL} , of the tungsten surface can be obtained by integrating the spectral emissivity, e_{PAL} , weighted with the plasma arc lamp irradiance, q_{i_L} as:

$$e_{PAL} = \grave{0}_{i_1}^{i_2} q_{i_i} e_i \, d \, I \, / \, \grave{0}_{i_1}^{i_2} q_{i_i} \, d \, I$$
 (1)

Using the spectral data presented in [23], and PAL irradiance, q_{i_l} [11, 22], e_{PAL} of tungsten at 1,100 K was estimated to be 0.47 over the plasma arc lamp spectrum. Thus, the net absorbed heat flux in tungsten would be, for the two PAL systems available, approximately 1.97 and 12.7 MW/m², respectively. On the other hand, it has to be mentioned that the tungsten surface will emit thermal radiation over the entire spectrum, i.e., not limited to the spectrum of the plasma arc lamp. The hemispherical *total* emissivity of W, e_{\downarrow} , is 0.14 at 1,100 K [24]. Assuming an emission from a gray body, the total heat flux into the tungsten material, from the top surface – including losses due to natural/forced convection and thermal radiation, is given as [22, 25]: $q'' = e_{PAL} q''_{PAL} - h_C (T - T_A) - S e_{\downarrow} (T^4 - T_A^4)$

where $q_{PAL}^{"}$, h_CT , T_A , S, are the incident heat flux from plasma arc lamp, heat transfer coefficient, surface temperature, ambient temperature, and Stefan-Boltzmann constant, respectively. This relationship indicate that as e_{\downarrow} is lower than e_{PAL} , the tungsten surface would be more effective

at absorbing heat from the plasma arc lamp than loosing heat to the ambient by thermal radiation. The value of the incident heat flux, $q_{PAL}^{"}$, was measured using a high-speed heat flux sensor [26]. The HFM-8E/H sensor from Vatell Corporation uses a thin film differential thermopile to measure heat flux and a type-E thin film thermocouple to simultaneously record the surface temperature and heat flux [27]. The heat flux was found to rise to approximately 80% of its peak in 0.02 s [22] and since the sensor has a response time of 0.3ms, this raise was not due to the sensor response time but to the actual start-up characteristic of the arc.

2.2. Design of Irradiated Material Target Station and diagnostics

In addition to the plasma arc lamps, the HHTF consists of an Irradiated Material Target Station (IMTS), as shown in Figure 2. The IMTS has been designed to accommodate the small-and-thin specimens, typical for high activity materials such as tungsten and rabbit iradiation capsules, and larger specimens required for the high-heat flux prototype component testing anticipated in the fusion program. Components of the test chamber and IMTS were designed by taking into account irradiation safety and materials compatibility requirements in order to handle the testing of low levels irradiated tungsten articles [11]. Irradiated specimens are to be placed in a shallow recess in the molybdenum holder that is attached to a water-cooled copper alloy rod (Figure 2b). In addition to the quartz plate on the top of the chamber, the molybdenum specimen holder on the top of the copper cooling rod assembly is enveloped by an end-capped cylindrical quartz tube (right photo) to confine any possible radioactive material released from irradiated specimen. Special considerations were devoted to the air evacuation from the test chamber and its backfilling with an inert atmosphere (Ar or Ar+4% H₂), which is necessary to avoid oxidation of tungsten articles at high temperatures. For ensuring safety in working with irradiated materials, the following steps were considered:

- 1. Ensure vacuum tightness of the IMTS using a high-temperture o-ring on the main quartz window to prevent the escape of irradiated gases during experiment,
- 2. Use a secondary inside IMTS to contain the specimen holder as a first containment area,
- 3. Install a pressure valve for regulating the pressure within the Al enclosure in order to prevent the pressure increase and eventual liftoff of the main quartz window during the high heat flux testing.

4. Measure the pressure inside the ITMS using a transducer during HHFT to detect any vacuum leaks during testing and stop the experiment during an accidental vacuum loss.

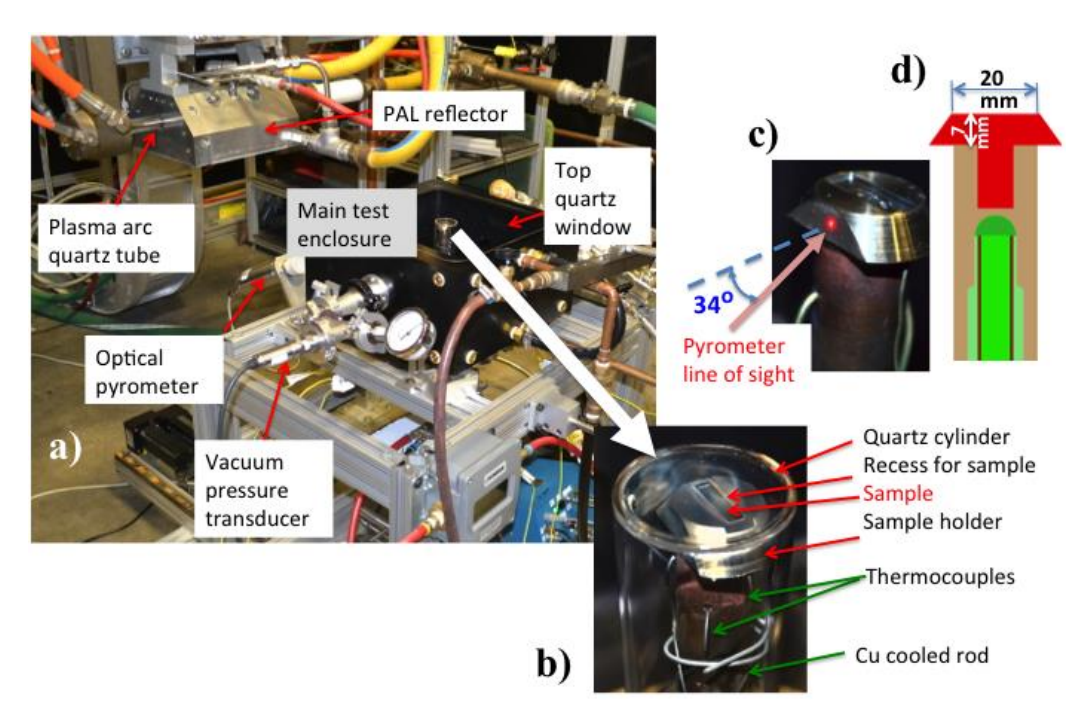


Figure 2. Experimental setup: (a) panoramic corner view showing major components of the system: arc lamp tube, PAL reflector, main Al (black anodized) enclosure, quartz window of top chamber, the pressure transducer, and pyrometer for in-situ surface temperature measurement of the Mo specimen holder, (b) test stand composed of quartz cylinder for containment of volatile irradiation gases, water cooled rod, holder, and thermocouples, (c) pyrometer spot size and direction with respect to the normal to the surface, and (d) schematic of the cooling rod and holder.

The following diagnostics were considered for the IMTS:

- water flow meter (12.6-126.2 cm³/s) to monitor the variation of coolant flow rate into the cooling rod and estimate cooling loads,
- optical pyrometer that was attached to the test section during in-situ measurements of the temperature of the Mo specimen holder,
- thermocouples embedded in the specimen holder, cooling rod, and outlet line.

Temperature control during high-heat IR testing of armor materials under fusion-prototypical steady state conditions is very important. For thin specimens which are often used for studies of neutron irradiation effects, one of the main challenges to the PAL systems is the measurement of the specimen temperature, since: (1) the PAL reflector is large enough to obstruct the specimen, precluding the use optical pyrometers due to the lack of the direct line of sight to the specimen, (2) the specimen cannot be bolted to the specimen holder, and (3) the thermocouples cannot be pushed against the specimen. In this respect, several molybdenum specimen holders were designed to vary the specimen temperature. In addition to the pyrometer that points to the side of the specimen holder, the Mo holder was instrumented with thermocouples that can be used to obtain the specimen temperature. Thus, the specimen temperature can be indirectly obtained using correlations between the specimen temperature and the other measured temperatures at various locations within the Mo holder, correlations that would be obtained either from calibration runs and/or numerical simulations.

3. Results of high-heat flux testing experiments

In this study, in a calibration run was first conducted when a thermocouple was welded to the back-side of a non-irradiated tungsten specimen, providing direct measurement of its temperature. For this calibration run, the specimen-reflector distance was 2 cm, the incident heat flux was about 3.2 MW/m² for 30 s, while the absorbed heat flux was into the specimen was approximately 1.6 W/m² (approx. 50% of the incident heat flux). Two holes were drilled in the Mo holder for insertion of thermocouples close to the backside surface of the specimen. The placement of thermocouple tips is shown for the sake of completion to aid in data interpretation (Figure 3a). Although not shown in Figure 4a for the sake of clarity, the closed hole for the thermocouple in the center of the specimen was opened for the calibration runs. The pyrometer aims at the specimen holder side (Figure 3b) at an angle of 34° with the respect to the normal direction to the specimen holder surface. The Mo holder has a conical surface and a cutout in order to reduce the heat flux absorbed in the testing fixture (Figure 2). The specimen temperature is showed in Figure 3(a) with open circle symbols. This data shows an actual increase from room temperature to 1,000s in the first 2 s. The data shown in Figure 3 indicate the following:

- 1) The pyrometer data is affected by the infrared energy from the PAL during high-energy pulses. The proof of artifact is the sharp raise and drop in pyrometer temperatures right at the onset and end of pulses. The fact that the temperature varies during the high energy indicates that the reflections from the PAL into the pyrometer, which creates the artifact at high-energies, is not dominant and thus it can be corrected.
- 2) The pyrometer data is not affected by the infrared energy during the idle period, after the end of high-energy pulses. The pyrometer temperature at idle has the similar temperature ranges as those measured by thermocouples inserted in the 1G Mo holder.

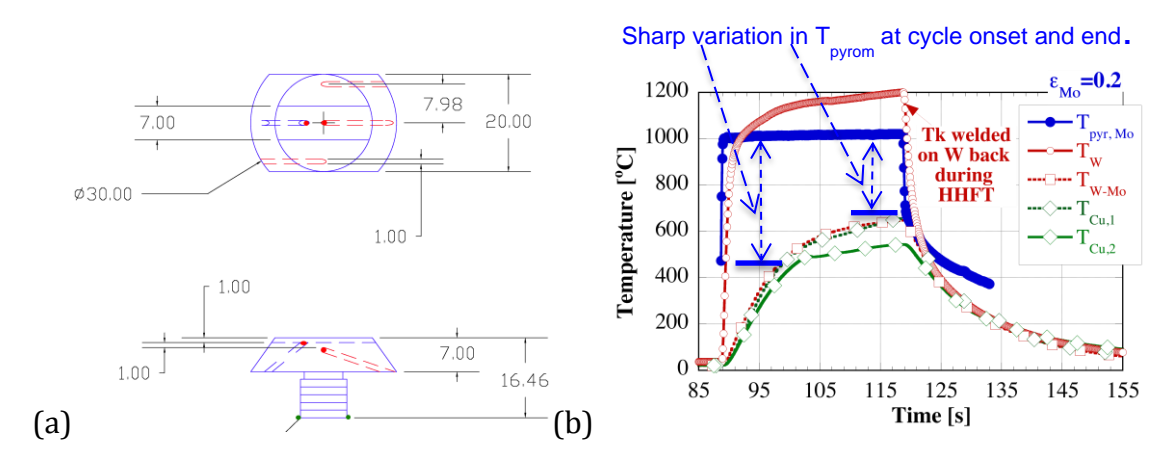


Figure 3. Data on HHFT of an non-irradiated specimen for calibration of specimen temperature: (a) 2-nd generation of Mo specimen holder dimensions (thermocouple tips close to the specimen are shown with red dots (b) Temperature measured by the pyrometer on the side surface of holder (T_{pyr,Mo}) thermocouple welded on tungsten specimen back surface during HHFT (T_W), thermocouple between tungsten specimen and holder (T_{W-Mo}), and thermocouples in the cooling rod at the ends of holder thread.

From the data shown in Figure 3, it is inferred that there would be a temperature difference between that measured by the pyrometer and that by the welded thermocouple on the backside of the tungsten specimen of approximately 490 and 400 °C, as estimated right when the pulse ended and 0.5 s after the pulse ended (to account for the pyrometer response time of 0.3s), respectively. On the other hand, there would also be a temperature difference of approximately 553 °C between the welded thermocouple and the thermocouple inserted in the open hole, but not welded to the specimen.

The first irradiated tungsten specimen S1 was exposed to 80 high-heat flux cycles while the second specimen, S2, was exposed to 200 cycles. For S1, the operating parameters of the HHFT were varied for the first several cycles such that the maximum thermocouple temperatures would be limited to 700 to 800 °C while allowing appropriate time for cooling (Table 1). According to the calibration data, this would translate into specimen temperatures of approximately 1,250 to 1,350 °C. The operating parameters include heat flux, duration of high-heat flux pulse, and duration of the idle period between pulses at 2% of the maximum heat flux. The measured temperatures using several thermocouples embedded in the specimen holder, as shown in Figure 3, are shown in Figure 4 with the estimated specimen temperatures shown in Figure 4. It has to be noted that the estimated specimen temperature using both thermocouple and pyrometer corrections are very close, validating our approach for reconstructing the specimen temperature. For the sake of brevity, only the data on first 80 cycles was shown in Figure 4 and 5 for the second specimen. Excluding the first two cycles for the first specimen, the estimated mean temperature of the peak specimen temperature was 1,314 and 1,309 °C when the pyrometer and thermocouple corrections were used, respectively, with the corresponding standard variations of 38 and 27 °C. For the second specimen, estimated mean temperature of the peak specimen temperature was 1,319 and 1,342 °C when the pyrometer and thermocouple corrections were used, respectively, with the corresponding standard variations of 41 and 15 °C.

Table. 1. Operating parameters of the HHFT for the specimen S1: incident heat flux – q" $[MW/m^2]$, pulse duration – τ_p [s], duration between pulses at idle power – τ_o [s].

Cycle	q"	$ au_p$	$ au_o$
	$[MW/m^2]$	[s]	[s]
]		
1	2.73	30	189
2	3.32	15	185
3	3.95	10	98
4	3.32	15	122
5	3.32	20	141
6	3.95	20	181
7	3.63	20	105
8	3.63	20	170

9	3.63	20	92
10	3.63	20	92
11	3.63	25	101
12	3.63	25	101
13	3.63	25	113
14-15	3.32	25	110
16-32	3.32	25	100
33-42	3.32	25	105
43-52	3.32	20	110
53-81	3.32	18	110

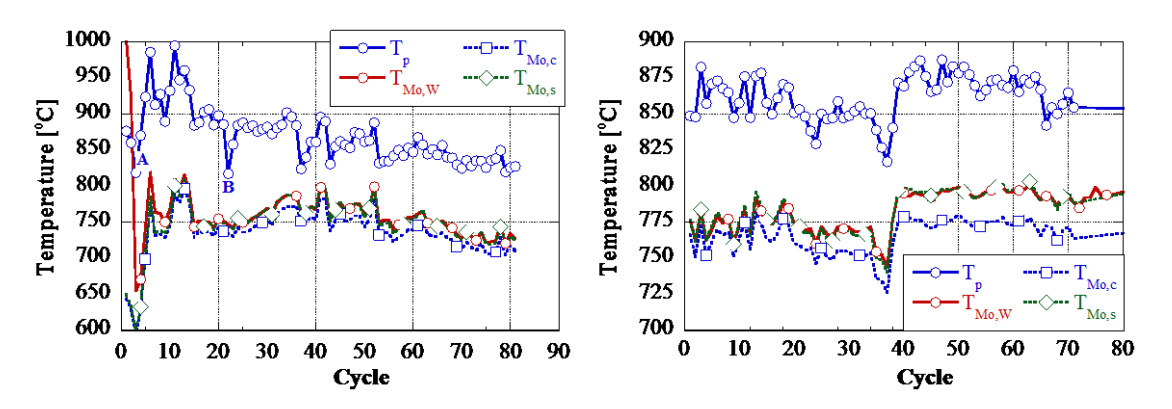


Figure 4. Peak temperatures per each cycle during HHFT for the irradiated specimens: (a) S1 exposed to 81 cycles and (b) S2 specimen exposed to 200 cycles. Temperature measured by the pyrometer on the side surface of Mo holder (T_p) , thermocouple on back surface of tungsten specimen in the open hole $(T_{Mo,W})$, thermocouple in the center of the specimen holder $(T_{Mo,c})$, and thermocouple on the side of the specimen holder $(T_{Mo,s})$.

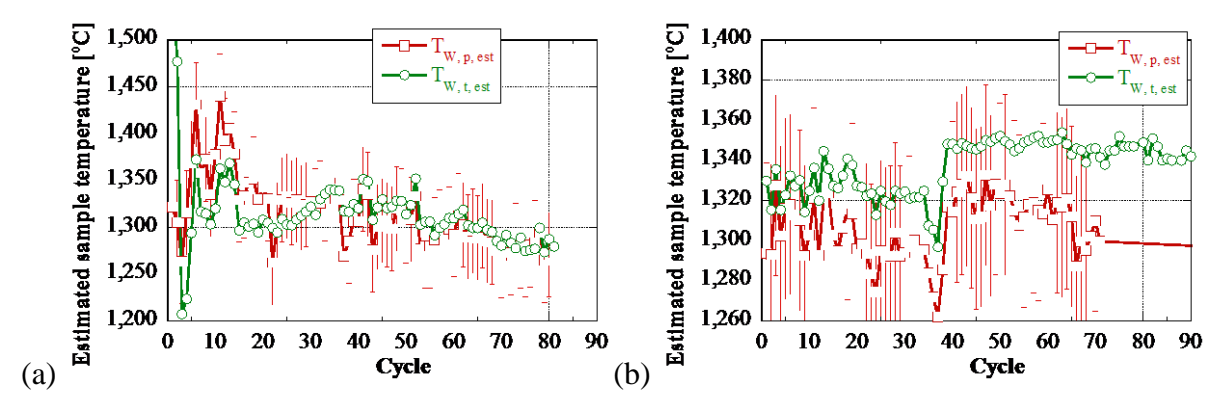


Figure 5. Estimated maximum temperature of the tungsten material for (a) specimen S1 and (b) specimen S2 (only 90 cycles out of 200 shown for the sake of clarity).

3.1 Contamination confinement

The HHFT were conducted in this study to assess the feasibility of the HHFT with the limited confinement of the test section. The entire contamination area is limited to IMTS size of 36x36x18 cm (length, width, height, respectively). Vacuum pressure was measured during the entire test in the IMTS and it was maintained during HHF testing at 27.45kPa, ensuring appropriate confinement of the contaminated gases within the IMTS. The standard deviation of the pressure variation was found to be 0.6 kPa during the high-heat flux exposure. The specimen

dose rates were 2,400 mrem/hr on contact and 20 mrem/h at 30 cm. After the specimens were placed in the specimen holder, the dose rates were 22 mrem/h at the quartz surface and 0.6 mrem/h at 30 cm. A contamination survey was conducted after the completion of each HHFT. Wipes, also known as smears, were used to estimate the levels of removable contamination. Even though large variations are expected in the smear contamination measurements, its relative variation between the two tests is noteworthy for comparison. For the testing of the first irradiated specimen, which was conducted in Ar atmosphere, the levels of contamination were highest on the bottom surface the IMTS (28,000 dpm/100 cm²-beta) and inside the quartz cylinder (3,800 dpm/Qtip) that was designed as a first level of containment. When the controlled atmosphere was changed to Ar + 4% H_2 for the second specimen, all the contamination surveys showed a consistent decrease in the contamination levels at all locations in the test section by a factor of five to ten.

4. Discussion

The implications of high-heat flux exposure on tungsten materials are now briefly discussed as this study was mainly focused on assessing the feasibility of the HHFT within the limited confinement of the test section. There were no mechanical stresses during HHFT in the thin and monolithic specimen tested in this study, as would be expected for real components. However, the temperature exposure is expected to affect the microstructure, in particular of material not subjected to a prior recrystallization anneal. The microstructure change depends on the time-temperature history of the specimen. In order to quantify the extent of annealing and its ensuing effects on properties, such as thermal conductivity, effective holding time, t_{eh} , at a given reference temperature, T_{ref} , is introduced as follows. t_{eh} is the time required to hold the specimen at a given reference temperature to attain the similar property changes as that during a non-isothermal exposure, such as that during a sequence of numerous HHF cycles, and is determined by:

$$t_{eh} \exp\left(-E_A / \left(kT_{ref}\right)\right) = \mathop{\circ}\limits_{0}^{t} \exp\mathop{\circ}\limits_{0}^{t} - E_A / \left(kT(t)\right) \mathop{\circ}\limits_{0}^{t} dt \text{ or } t_{eh} = \mathop{\circ}\limits_{i=1}^{N} t_{p,i} \exp\mathop{\circ}\limits_{0}^{t} E_a \left(1/T_i - 1/T_{ref}\right) / k \mathop{\circ}\limits_{0}^{t}$$
(3)

where k is the Boltzmann's constant, 8.314 J/mole-K, E_A =362.5 kJ/mol is the activation energy for the recrystallization of pure tungsten [28], $E_A/k = 4.36 \times 10^4 \text{K}$, T_i [K] is the peak temperature for i-th

cycle, whose pulse duration is $\tau_{p,i}$ [s], and N is the total number of pulses. Considering $T_{ref} = 1,300^{\circ}\text{C}$ (1,573K). Other diffusion-based phenomena, such as thermal conductivity changes of irradiated materials, may be able to be described by the same formalism [29]. Neglecting the 2 s time raise to over 1,000 °C C during a typical cycle (Figure 3b), the residence time at peak temperature (above 1,000 °C), was estimated to be approximately 1,580 and 3,604 s for the first and second specimen, respectively. The t_{eh} was calculated using formula 3, using the actual peak temperatures for each cycle to be 1,395 and 1,805 s for the first and second specimen, respectively. If the deformation of these specimens had restrained during HHFT, then the ensuing state of stress and strain would have affected the recrystallization. When a first order approximation was used, using the average residence times and mean value for the peak cycle temperatures, the t_{eh} were estimated to be approximately 1,350 and 1,753 s for the first and second specimen, respectively; resulting in an underestimating of t_{eh} by 50 s for both specimens, which is approximately 2.7 to 3.6 % error.

Conclusions

High-heat flux tests of neutron irradiated tungsten specimens were conducted. The experiments were conducted in a controlled atmosphere, Ar and Ar+4% H₂. Radiological surveys indicated minimal contamination of the 36x36x18 cm test section, demonstrating the capability of the new facility to handle irradiated specimens at high temperature. One of the most difficult tasks was the measurement of specimen temperature, especially for thin and monolithic specimens, which are often used for studies of neutron irradiation effects. The best data on specimen temperature was obtained as a thermocouple welded during the high-heat flux testing. The implications of high-heat flux exposure on tungsten materials were briefly discussed as this study was mainly focused on assessing the feasibility of the HHFT using high-energy waterwall plasma-arc-lamps within the limited confinement of the test section. The use of the high-heat flux testing facility using Plasma Arc Lamps was demonstrated at ORNL for low levels of irradiated tungsten specimens within a very small contamination volume. This new high-heat flux testing facility will be used to study the behavior of irradiated materials as exposed to high-heat fluxes relevant to ITER conditions.

Acknowledgments

This work was supported by Office of Fusion Energy Sciences, U.S. Department of Energy

under contract DE-C05-00OR22725 with UT-Battelle, LLC and "Technological Assessment of Plasma Facing Components for DEMO Reactors" Japan/U.S.A. Fusion Research joint project. The authors would like to thank Dr. Michael Rieth and Dr. Jens Reiser of Karlsruhe Institute of Technology, Germany for providing the tungsten specimens and Ms. Marie Alta Williams of ORNL for safety considerations related to the neutron irradiated materials and Ms. Stephanie Curlin of ORNL for taking the micrographs.

References

- [1] T. Hirai, K. Ezato, P. Majerus, Materials Transactions, Vol. 46, No.3, 412 (2005)
- [2] T. Hirai, H. Maier, M. Rubel, Ph. Mertens, R. Neu, E. Gauthier, J. Likonen, C. Lungu, G. Maddaluno, G.F. Matthews, R. Mitteau, O. Neubauer, G. Piazza, V.Philipps, B. Riccardi, C. Ruset, I. Uytdenhouwen, JET EFDA Contributors, Fusion Eng. and Design, Vol. 82, pp. 1839-1845, 2007.
- [3] S. Suzuki; Suzuki, T.; Nakamura, K.; Akiba, M., Fusion Eng., 1997. 17th IEEE/NPSS Symposium, Vol. 1, pp. 385-388, 1997.
- [4] R.C. Rau, J. Moteff and R. L. Ladd, J. Nucl. Mater., Vol. 24, pp. 164–173, 1967.
- [5] J. M. Steichen, J. Nucl. Mater., Vol. 60, pp. 13-19, 1976.
- [6] I.V. Gorynin; Ignatov, VA; Rybin, VV; Fabritsiev, SA; Kazakov, VA; Chakin, VP; Tsykanov, VA; Barabash, VR; and Prokofyev, YG, J. Nucl. Mater., Vol. 191, pp. 421-425, 1992.
- [7] V.R. Barabash, Federici, G; Rodig, M; Snead, LL and Wu, CH, J. Nucl. Mater., Vol. 283, pp. 138-146, 2000.
- [8] T.S. Byun and K. Farrell, J. Nucl. Mater., Vol. 326, pp. 86-96, 2004.
- [9] G. Romanoski, L. Snead, A. Sabau, J. Kelly, S. Zinkle ,*HAPL Workshop*, LLNL, June 20-21, 2005.
- [10] T. Hinoki, L. L. Snead, and C. Blue. J. Nucl. Mater., Vol. 347, pp. 207-216, 2005.
- [11] Sabau A.S., Ohriner E.K., Kiggans J.O., Harper D.C., and Snead L.L., "Facility for high heat flux testing of irradiated fusion materials and components using infrared plasma arc lamps" accepted for publication in the Physica Scripta, Oct., 2013.
- [12] M. Rieth, A. Hoffmann, Sept. 28-Oct. 2, San Francisco, CA (TOFE-18), 2008.
- [13] M. Rieth, A. Hoffmann, Int. Journal of Refractory Metals and Hard Materials, Vol., 28, pp. 679–686, 2010.

- [14] M. Faleschini, H. Kreuzer, D. Kiener, R. Pippan, J. Nucl. Mater., Vol. 367, pp. 800–805, 2007.
- [15] T.S. Byun, K. Farrell, N. Hashimoto, J. Nucl. Mater., Vol. 329-333, Part B, pp. 998-1002, 2004.
- [16] A. Hasegawa, T. Tanno, S. Nogami, M. Satou, J. Nucl. Mater., Vol. 417, pp. 491-494, 2011.
- [17] J. Reiser, M. Rieth, B. Dafferner, A. Hoffmann, X. Yi, D. E.J. Armstrong, J. *Nucl.* Mater., 424 (2012) 197–203.
- [18] R.A. Nodwell and D.M. Camm, US Patent 4,027,185, High intensity radiation source, Canadian Patents and Development Limited, 05/31/1977.
- [19] D.M. Camm; A. Kjorvel; N.P. Halpin, A. J.D. Housden, US Patent 4,700,102, High intensity radiation apparatus having vortex restriction means, Vortek Industries, Ltd., 10/13/1987.
- [20] D.M. Camm, US Patent, 4,683,525, Lamp having segmented reflector, Fusion Systems Corporation, 07/28/1987.
- [21] T. Thrum, D. Camm, S. Dets, A. Hewett, I. Rudic, G.S. Stuart, A. Viel, in IEEE Industry Applications Conference 2004, Seatle, WA, pp. 1019-1023.
- [22] A.S. Sabau, C.E. Duty, R.B. Dinwiddie, M. Nichols, C.A. Blue, and R.D. Ott, J. Appl. Phys. 105, 084901 (2009), DOI:10.1063/1.3097356.
- [23] S. Roberts, Phys. Rev. 114, 104–115 (1959).
- [24] T. Matsumoto, A. Cezairliyan, D. Basak, Int. J. Thermophys. Vol. 20-3, pp. 943-952, 1999.
- [25] J. D. K. Rivard, A.S. Sabau, C. A. Blue, E. K. Ohriner, N. Jayaraman, *Metall. and Mat.Trans. A*, 2003 Vol. 34A, pp. 3043-3054.
- [26] A.S. Sabau and Z.X. Wu, Journal of Materials Processing Technology, 182, 312-318 (2006).
- [27] J.M. Hager, L.W. Langley, S. Onishi, and T. E. Diller, J. Thermophys. Heat Transfer, Vol. 7, pp. 531 (1993).
- [28] T. Zhang, Y. Wang, Y. Zhou, T. Lei, and G. Song, Journal of Mater. Sci., Vol. 41, pp. 7506-7508, 2006, DOI: 10.1007/s10853-006-0834-9
- [29] A.S. Sabau, J.K.D. Rivard, C.A. Blue, E.K. Ohriner, and D.C. Harper, Int. Thermal Conductivity Conf. 27, Knoxville, TN, October 29, 2003, Ed. H. Wang and W. Porter, DEStech Publications, Inc., Lancaster, PA, pp. 511-521.